

Gamow-Teller transitions to ^{45}Ca via the $^{45}\text{Sc}(t, ^3\text{He} + \gamma)$ reaction at 115 MeV/ u and its application to stellar electron-capture rates

S. Noji,^{1,2,*} R. G. T. Zegers,^{1,2,3} Sam M. Austin,^{1,2} T. Baugher,^{1,3,†} D. Bazin,¹ B. A. Brown,^{1,2,3} C. M. Campbell,⁴ A. L. Cole,^{2,5} H. J. Doster,^{1,3} A. Gade,^{1,3} C. J. Guess,^{6,‡} S. Gupta,⁷ G. W. Hitt,⁸ C. Langer,^{1,2,§} S. Lipschutz,^{1,2,3} E. Lunderberg,^{1,3} R. Meharchand,^{9,||} Z. Meisel,^{1,2,3} G. Perdikakis,^{1,2,10} J. Pereira,^{1,2} F. Recchia,^{1,¶} H. Schatz,^{1,2,3} M. Scott,^{1,3} S. R. Stroberg,^{1,3,#} C. Sullivan,^{1,2,3} L. Valdez,¹¹ C. Walz,^{1,**} D. Weisshaar,¹ S. J. Williams,¹ and K. Wimmer^{1,10,††}

¹National Superconducting Cyclotron Laboratory, Michigan State University, East Lansing, Michigan 48824, USA

²Joint Institute for Nuclear Astrophysics, Michigan State University, East Lansing, Michigan 48824, USA

³Department of Physics and Astronomy, Michigan State University, East Lansing, Michigan 48824, USA

⁴Lawrence Berkeley National Laboratory, Berkeley, California 94720, USA

⁵Physics Department, Kalamazoo College, Kalamazoo, Michigan 49006, USA

⁶Department of Physics and Applied Physics, University of Massachusetts Lowell, Lowell, Massachusetts 01854, USA

⁷Indian Institute of Technology Ropar, Nangal Road, Rupnagar, Punjab 140001, India

⁸Department of Applied Mathematics and Sciences, Khalifa University of Science, Technology, and Research, P.O. Box 127788 Abu Dhabi, UAE

⁹Neutron and Nuclear Science Group, Los Alamos National Laboratory, Los Alamos, New Mexico 87545, USA

¹⁰Department of Physics, Central Michigan University, Mt. Pleasant, Michigan 48859, USA

¹¹Orange High School, Orange, New Jersey 07050, USA

(Received 19 March 2015; published 17 August 2015)

Background: Stellar electron-capture reactions on medium-heavy nuclei are important for many astrophysical phenomena, including core-collapse and thermonuclear supernovae and neutron stars. Estimates of electron-capture rates rely on accurate estimates of Gamow-Teller strength distributions, which can be extracted from charge-exchange reactions at intermediate beam energies. Measured Gamow-Teller transition strength distributions for stable pf -shell nuclei are reasonably well reproduced by theoretical calculations in the shell model, except for lower mass nuclei where admixtures from the sd shell can become important.

Purpose: This paper presents a β^+ charge-exchange experiment on ^{45}Sc , one of the lightest pf -shell nuclei. The focus was on Gamow-Teller transitions to final states at low excitation energies, which are particularly important for accurate estimations of electron-capture rates at relatively low stellar densities. The experimental results are compared with various theoretical models.

Method: The double-differential cross section for the $^{45}\text{Sc}(t, ^3\text{He} + \gamma)$ reaction was measured using the NSCL Coupled-Cyclotron Facility at 115 MeV/ u . Gamow-Teller contributions to the excitation-energy spectra were extracted by means of a multipole-decomposition analysis. γ rays emitted due to the deexcitation of ^{45}Ca were measured using GRETTINA to allow for the extraction of Gamow-Teller strengths from very weak transitions at low excitation energies.

Results: Gamow-Teller transition strengths to ^{45}Ca were extracted up to an excitation energy of 20 MeV, and that to the first excited state in ^{45}Ca at 174 keV was extracted from the γ -ray measurement, which, even though weak, is important for the astrophysical applications and dominates under certain stellar conditions. Shell-model calculations performed in the pf shell-model space with the GXPF1A, KB3G, and FPD6 interactions did not reproduce the experimental Gamow-Teller strength distribution, and a calculation using the quasiparticle random phase approximation that is often used in astrophysical simulations also could not reproduce the experimental strength distribution.

Conclusions: Theoretical models aimed at describing Gamow-Teller transition strengths from nuclei in the lower pf shell for the purpose of estimating electron-capture rates for astrophysical simulations require further development. The likely cause for the relatively poor performance of the shell-model theory is the influence of intruder configurations from the sd shell. The combination of charge-exchange experiments at intermediate beam energy and high-resolution γ -ray detection provides a powerful technique to identify weak transitions to low-lying final states that are nearly impossible to identify without the coincidences. Identification of these weak low-lying transitions is important for providing accurate electron-capture rates for astrophysical simulations.

DOI: [10.1103/PhysRevC.92.024312](https://doi.org/10.1103/PhysRevC.92.024312)

PACS number(s): 23.40.-s, 25.55.Kr, 26.30.Jk, 27.40.+z

*noji@renp.osaka-u.ac.jp; present address: Research Center for Nuclear Physics, Osaka University, Ibaraki, Osaka 567-0047, Japan.

†Present address: Department of Physics and Astronomy, Rutgers University, Piscataway, New Jersey 08854, USA.

‡Present address: Department of Physics and Astronomy, Swarthmore College, Swarthmore, PA 19081, USA.

§Present address: Goethe-Universität Frankfurt am Main, D-60438 Frankfurt am Main, Germany.

I. INTRODUCTION

Electron-capture (EC) reactions on medium-heavy nuclei play a significant role in many astrophysical phenomena [1] such as core-collapse (type II) supernovæ (SNe) [1–5], thermonuclear (type Ia) SNe [6,7], and heating [8] and cooling [9] processes in crusts of accreting neutron stars. The estimation of EC reaction rates requires knowledge of Gamow-Teller (GT) strength [$B(\text{GT})$] distributions in the β^+ direction. Typically a large number of nuclei, including some that are unstable, play a role. Moreover, in stellar environments, the temperature can be sufficiently high to populate excited states in nuclei, on which EC can occur as well. Since it is impossible to measure all relevant GT transitions, experiments must focus on comprehensively benchmarking theoretical approaches and on nuclei that are particularly important for specific astrophysical processes.

Experimental GT strengths can be obtained from β -decay measurements, but such measurements are limited to an often small Q -value window, if they are feasible at all. Charge-exchange (CE) reactions at intermediate beam energies ($\gtrsim 100$ MeV/ u) can provide full $B(\text{GT})$ distributions based on the well-established proportionality between the CE cross section at zero momentum transfer and $B(\text{GT})$ [10–12]. In Refs. [13] and [14], a systematic study of the EC rates was performed for 13 stable pf -shell nuclei with $45 \leq A \leq 64$ based on CE data from (n, p) , $(d, ^2\text{He})$, and $(t, ^3\text{He})$ experiments for which the locations of daughter states at low excitation energies have been well established. It was found that experimental GT strength distributions and derived EC rates are generally reproduced quite well in shell-model (SM) calculations using the GXPF1A [15–17] and the KB3G [18] interactions. A study of GT strengths from ^{56}Ni [19,20] indicated that the SM calculations with the GXPF1A interaction perform slightly better than the SM calculations with the KB3G interaction. Calculations based on the quasiparticle random phase approximation (QRPA) formalism of Ref. [21] performed worse than either SM calculations. These QRPA calculations, as well as the SM calculations using the KB3G interaction, are regularly used in astrophysical simulations that require EC rates.

For specific nuclei, significant discrepancies between experiments and SM calculations were observed [13], especially for GT excitations to low-lying final states. Such transitions are the most important for the accurate estimation of EC rates in astrophysical phenomena, especially at lower stellar densities and temperatures. In a recent study of the $(t, ^3\text{He})$ reaction on the nucleus ^{46}Ti [22] significant deficiencies in SM calculations based on the GXPF1A, KB3G, and FPD6 [23] effective interactions for the pf shell were observed. It is likely

due to admixtures from protons and neutrons in the sd -shell configurations which are not included in the SM calculations, which assume a closed ^{40}Ca core. It was concluded that further improvements to the theoretical calculations of GT strengths for nuclei in the lower pf shell are needed.

In the present study, we investigated nearby ^{45}Sc , which is one of the lightest pf -shell nuclei, by measuring the $B(\text{GT})$ distribution via the $^{45}\text{Sc}(t, ^3\text{He})$ reaction. Under the assumption of a closed ^{40}Ca core, ^{45}Sc is one of the simplest pf -shell nuclei with nonvanishing first-order β^+ GT strength since it has only one proton in the pf shell. Hence, it is an attractive case to further investigate possible admixtures from sd -shell configurations. We have applied the same technique as used for the investigation of ^{46}Ti [22], namely a CE reaction measurement in combination with high-resolution γ -ray detection from the excited residue. This enables one to perform detailed spectroscopy since one can gate on a specific excitation energy in the $(t, ^3\text{He})$ spectrum and investigate the γ decays without ambiguities related to feeding from higher-lying states. Note that it is clear that one cannot pinpoint a single, or even a few, nuclei that are critical for the relevant astrophysical scenarios. The approach followed here is to provide detailed data that will guide the development of theoretical models in a deliberate manner. Specifically, the focus is on providing such guidance for nuclei just above the sd shell-model space.

The GT strength distribution from ^{45}Sc to ^{45}Ca had been previously extracted in an (n, p) measurement at 198 MeV at TRIUMF [24]. The relatively poor energy resolution of that measurement (~ 1 MeV in FWHM) made it difficult to make a detailed comparison between the data and theory. In the present work, the $^{45}\text{Sc}(t, ^3\text{He})$ reaction at an incident triton energy of 115 MeV/ u was used to extract the GT strength distribution with better resolution, which, together with the high-resolution coincidence measurement of the deexcitation γ -ray from the residue, allowed for a more precise comparison between data and theory and made it possible to include the case of ^{45}Sc in the evaluation of theoretical EC rates for pf -shell nuclei as presented in Refs. [13,14].

II. EXPERIMENT

The measurement was carried out at the Coupled Cyclotron Facility at the National Superconducting Cyclotron Laboratory. A 150-MeV/ u beam of ^{16}O with an intensity of 150 pA impinged on a 3525-mg/cm²-thick beryllium target, and tritons at 115 MeV/ u were selected from various fragmentation products in the A1900 fragment separator [25] with a 195-mg/cm²-thick wedge-shaped aluminum degrader at the intermediate image [26]. About 5×10^6 tritons (^3H) per second with a purity in excess of 99% were transported by using the dispersion-matching technique [27,28] to a ^{45}Sc reaction target with a thickness of 9.1 mg/cm² and with dimensions of $2'' \times 3''$.

The ^3He ejectiles from the target were magnetically momentum-analyzed by the S800 spectrometer [29], and detected at the focal plane by two cathode-readout drift chambers (CRDCs) [30]. A 5-mm-thick plastic scintillation counter was also placed at the focal plane of the S800 and

^{||}Present address: Institute for Defense Analyses, Alexandria, VA 22311, USA.

[¶]Present address: Dipartimento di Fisica e Astronomia, Università degli Studi di Padova, I-35131 Padova, Italy.

[#]Present address: TRIUMF, Vancouver, British Columbia V6T 2A3, Canada.

^{**}Present address: Institut für Kernphysik, Technische Universität Darmstadt, D-64289 Darmstadt, Germany.

^{††}Present address: Department of Physics, University of Tokyo, Bunkyo, Tokyo 113-0033, Japan.

enabled particle identification of the ^3He ejectiles through a combination of energy-loss and time-of-flight information.

For each event, the scattering angle and momentum of the ^3He particle at the target were reconstructed from the position and angle measured at the focal plane of the S800. The excitation energy in ^{45}Ca was obtained from a missing-mass calculation. Absolute double-differential cross sections, $d^2\sigma/d\Omega dE$, were determined relative to those of the $^{12}\text{C}(t, ^3\text{He})^{12}\text{B}(1^+, \text{g.s.})$ reaction, taken with a polyethylene (CH_2) target with a thickness of 10 mg/cm^2 , for which absolute cross sections were measured accurately in a previous experiment [12]. The double-differential cross sections were determined for the excitation-energy range of $0 \leq E_x \lesssim 20 \text{ MeV}$ and the scattering-angle range of $0^\circ \leq \theta_{\text{c.m.}} \lesssim 6^\circ$. The energy and angular resolutions were estimated from the same $^{12}\text{C}(t, ^3\text{He})$ spectra; they were 0.3 MeV and 1.0° , FWHM, respectively. The background due to hydrogen contamination in the ^{45}Sc target was evaluated and subtracted by using the corresponding peak in the $^1\text{H}(t, ^3\text{He})$ spectra also taken with the same CH_2 target.

The high-purity germanium detector array GREINA [31], located at the target position of the S800, was used for detecting deexcitation γ rays from the ^{45}Ca residue. The use of GREINA allowed precise determination of γ -ray energies. The large detector volume provided a high photopeak detection efficiency, and its high peak-to-total ratio enabled the measurement of low-yield transitions, including weak GT transitions at low excitation energies.

III. RESULTS AND ANALYSIS

Double-differential cross sections for the $^{45}\text{Sc}(t, ^3\text{He})$ reaction are shown in the left panel of Fig. 1. Note that wider energy bin sizes were used at higher excitation energies to reduce the statistical uncertainties. The systematic uncertainty in the absolute normalization of the cross section was estimated to be 6%, which was dominated by the uncertainty in the triton beam intensity. The intensity was monitored by calibrating the current readout for the unreacted ^{16}O beam in a Faraday bar placed in the first dipole magnet of the A1900 fragment separator against the aforementioned absolute cross section for the $^{12}\text{C}(t, ^3\text{He})^{12}\text{B}(1^+, \text{g.s.})$ reaction. The systematic uncertainties introduced by the subtraction of the background reactions on hydrogen instead of ^{45}Sc were small compared to those introduced by the beam intensities.

A. Multipole-decomposition analysis

A multipole-decomposition analysis (MDA) [32,33] was performed to extract the $\Delta L = 0$ (GT) components from the measured differential cross sections. The method used here was similar to the one described in Ref. [33]. The angular distribution in each bin of the excitation energy, $E_x(^{45}\text{Ca})$, was fitted with a linear combination of angular distributions calculated in the distorted-wave Born approximation (DWBA) with $\Delta L = 0, 1, 2$, and 3. The calculations were performed with the microscopic, double-folding DWBA code FOLD/DWHI [34]. The single-particle wave functions for t and ^3He were taken from variational Monte Carlo calculations [35], and those for

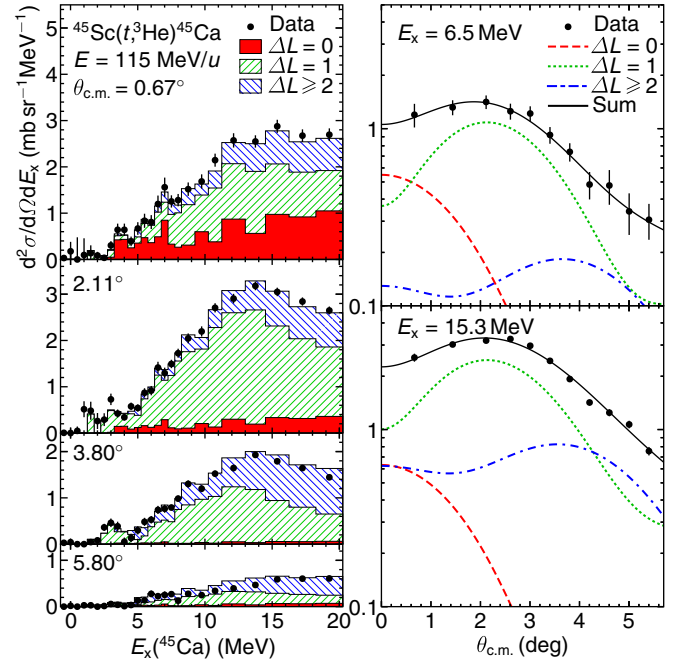


FIG. 1. (Color online) (Left) Double-differential cross section spectra for the $^{45}\text{Sc}(t, ^3\text{He})$ reaction at various scattering angles. The error bars denote the statistical uncertainty only. The histograms also show the results from the multipole-decomposition analysis (MDA). (Right) Representative angular distributions at $E_x = 6.5$ and 15.3 MeV including the results from the MDA.

^{45}Sc and ^{45}Ca were generated by using a Woods-Saxon potential. The effective NN interaction at 140 MeV of Ref. [36] was used. The optical-model-potential (OMP) parameters were taken from the $^3\text{He} + ^{58}\text{Ni}$ reaction at 443 MeV in Ref. [37]. Following Ref. [38], the depths of the OMPs for the triton in the incoming channel were scaled from those for the ^3He in the outgoing channel by a factor of 0.85 . The results of the MDA are also shown in the left panel of Fig. 1. It can be seen that the extracted $\Delta L = 0$ contributions are consistent with zero up to an excitation energy of about 3 MeV . As shown by two examples in the right panels of Fig. 1, the experimental angular distributions are well reproduced in the MDA. The statistical error of the MDA was estimated by means of a Monte Carlo simulation, as described in Ref. [39], where the experimental data points were randomly varied in accordance with their statistical uncertainty, and the deviation of the resulting $\Delta L = 0$ cross section was determined. A systematic error was estimated by using other trials of the MDA with different OMP as described in Ref. [40]. The extracted $\Delta L = 0$ components varied by less than 5%. The uncertainties in the extraction of the $\Delta L = 0$ contribution above $E_x = 10 \text{ MeV}$ is very large, partly because its contribution to the total cross section becomes relatively small while the statistical uncertainties are significant. In addition, in this higher energy region, the forward-peakedness of the angular distribution of the $\Delta L = 0$ cross section becomes somewhat less distinct. This was also the case in the previous $^{46}\text{Ti}(t, ^3\text{He})$ study [22]. Also note that contribution from the excitation of the isovector spin-monopole resonance (IVSMR) [39,41,42] is expected for $E_x \gtrsim 15 \text{ MeV}$.

B. Extraction of GT strengths

The $B(\text{GT})$ was calculated from the extracted $\Delta L = 0$ cross sections at 0° [$\sigma_{\Delta L=0}(0^\circ)$] by using the proportionality relation [10–12] between $\sigma_{\Delta L=0}(0^\circ)$ and $B(\text{GT})$,

$$\sigma_{\Delta L=0}(0^\circ) = \hat{\sigma}_{\text{GT}} F(q, \omega) B(\text{GT}), \quad (1)$$

where $\hat{\sigma}_{\text{GT}}$ is the GT unit cross section and $F(q, \omega)$ is a kinematical correction factor representing the dependence of $\sigma_{\Delta L=0}(0^\circ)$ on the momentum (q) and the energy (ω) transfers. The $\hat{\sigma}_{\text{GT}}$ for the $(t, {}^3\text{He})$ and $({}^3\text{He}, t)$ reactions at this energy have been calibrated in a systematic study [12], and is $\hat{\sigma}_{\text{GT}} = 109A^{-0.65} \text{ mb sr}^{-1}$ with A being the mass number of the target nucleus. The value $\hat{\sigma}_{\text{GT}}|_{A=45} = 9.18 \text{ mb sr}^{-1}$ was used for the present analysis, and this value has an uncertainty of about 10% [12]. $F(q, \omega)$ was calculated using the DWBA.

The extracted $B(\text{GT})$ distribution is shown in Fig. 2. In Fig. 2(a), a comparison of the $B(\text{GT})$ distributions of the present work and of the previous (n, p) work [24] is shown. They agree within about a factor of two with each other except for the excitation-energy range below 3 MeV, where the $B(\text{GT})$ values are consistent with zero in the present work. This discrepancy is likely due to the contribution from reactions on hydrogen absorbed onto the ${}^{45}\text{Sc}$ target in the case of the (n, p) experiment. As the authors of Ref. [24] noted, contributions from reaction on hydrogen would interfere with the spectrum at low excitation energies, but could not be subtracted. They therefore concluded that their results in the excitation-energy region below 3 MeV provided only an upper limit. We note that the $B(\text{GT})$ for the transition from the ${}^{45}\text{Sc}$ ($J^\pi = 7/2^-$) ground state to the ${}^{45}\text{Ca}$ ($J^\pi = 7/2^-$) ground state is known from the corresponding β decay, with the $\log ft$ value of 6.0 [43] which corresponds to a $B(\text{GT})$ value of 3.8×10^{-3} . The cross section associated with such a $B(\text{GT})$ is too small to be observable as a distinct peak in our data.

C. Analysis of coincidence γ rays

The analysis of the γ rays provided more detailed information on the low-lying states. We analyzed the data in a similar way as in the preceding paper (Ref. [22]). Figure 3(a) is a two-dimensional plot of the γ -ray energy (E_γ) measured with GREINA and the excitation energy $E_x({}^{45}\text{Ca})$ extracted from the $(t, {}^3\text{He})$ data. A sharp boundary along the $E_\gamma = E_x$ line is seen, which indicates that the spectrum is nearly background-free. A clear drop of the γ -ray yield at the neutron separation energy ($S_n = 7414.79 \text{ keV}$) is also observed. In the present case, the ground state of ${}^{45}\text{Ca}$ ($J^\pi = 7/2^-$) is reached by a GT transition from ${}^{45}\text{Sc}$ ($J^\pi = 7/2^-$). After the ${}^{45}\text{Ca}$ ground state, the next known state is located at 174.25 keV, which has $J^\pi = 5/2^-$ and is thus reachable by a GT transition [44]. It should also be noted that the next state above 174 keV reachable by a GT transition, based on the assigned J^π , does not appear until 1973(6) keV ($J^\pi = 5/2^-$ or $7/2^-$) [44].

The 174-keV state has a branching of 100% for γ decay to the ground state. Figure 3(b) is the γ -ray energy spectrum gated on $E_x = 174 \pm 380 \text{ keV}$ in the ${}^{45}\text{Sc}(t, {}^3\text{He})$ excitation energy spectrum, where the width of the gate corresponds to 3σ of the excitation energy resolution. Since other states that

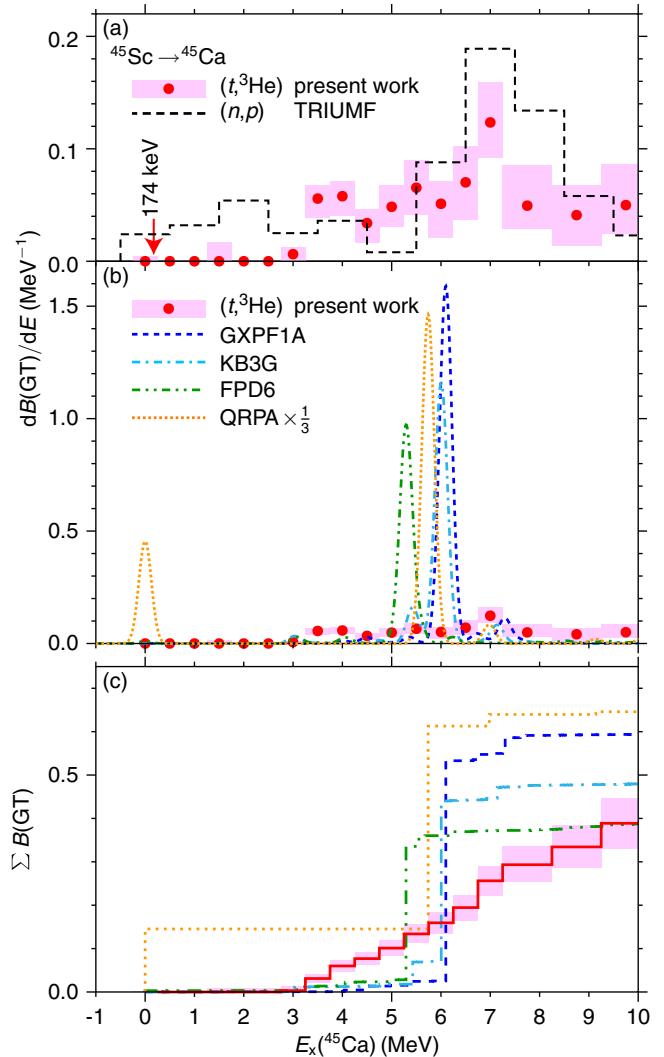


FIG. 2. (Color online) (a) $B(\text{GT})$ distribution extracted in the MDA of the ${}^{45}\text{Sc}(t, {}^3\text{He})$ data. The error bars denote the statistical and systematic uncertainties. The $B(\text{GT})$ distribution extracted from the (n, p) data at 198 MeV [24] is also shown for comparison. (b) $B(\text{GT})$ distribution from the $(t, {}^3\text{He})$ data is compared with the SM calculations with the GXPF1A, KB3G, and FPD6 interactions and with the QRPA calculation smeared with the experimental resolution. The results from the QRPA calculation are divided by a factor of 3. (c) Cumulative sum of the $B(\text{GT})$ distribution from the $(t, {}^3\text{He})$ data and those from the theoretical calculations.

are potentially excited and contained in this gate do not decay through the 174-keV state, the observation of events with the 174-keV γ ray in Fig. 3(b) directly relates to the excitation of the 174-keV state. The number of counts with $E_\gamma = 174 \text{ keV}$ in Fig. 3(b) can be converted to the GT strength of this state after taking into account the detection efficiency of GREINA. The obtained $B(\text{GT})$ of this state was 0.008(5), where the uncertainty is a combination of the statistical and systematic contributions. A systematic error of 0.003 due to interference effects between $\Delta L = 0$, $\Delta S = 1$, and $\Delta L = 2$, $\Delta S = 1$ amplitudes mediated through the tensor interaction [10] was estimated based on previous studies [45,46]. Such interference

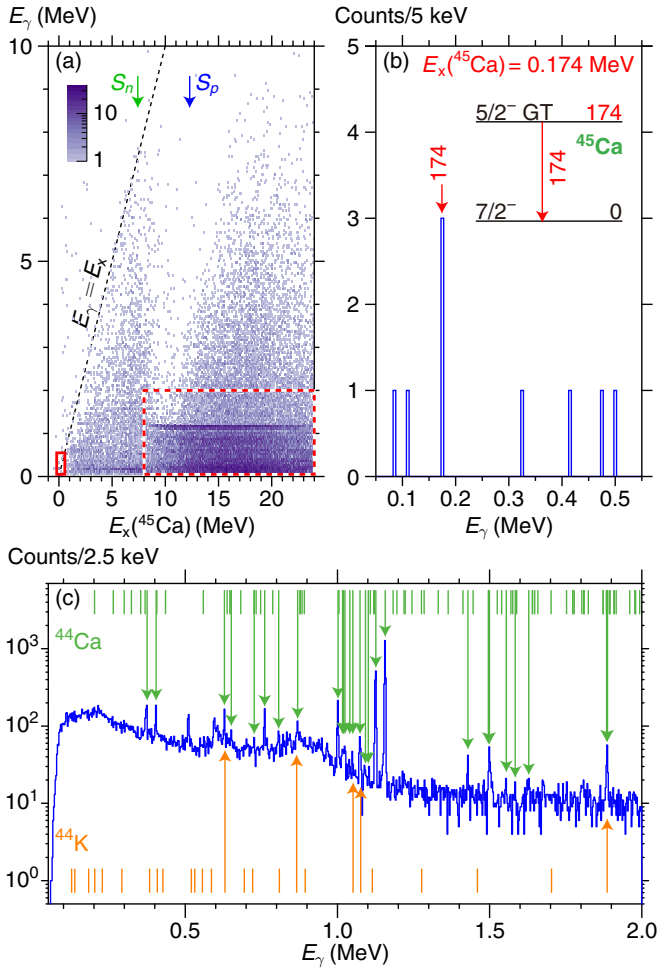


FIG. 3. (Color online) (a) E_γ vs $E_x(^{45}\text{Ca})$. The $E_\gamma = E_x$ line is shown, and the proton (S_p) and neutron (S_n) separation energies are also indicated. (b) A projection of (a) onto the E_γ axis, gated on $E_x(^{45}\text{Ca})$ around 174 keV as indicated by the box in (a). The inset shows a schematic decay diagram of the 174-keV state. (c) E_γ spectrum gated on $E_x > 8$ MeV. The selected region is indicated by the dashed rectangle in (a). The known γ -ray energies [47] are indicated, with the matched peaks shown by arrows.

effects can be relatively large for very weak GT transitions. Reliable strength of such a weak transition could not have been extracted without the coincident high-resolution measurement of γ rays.

Figure 3(c) shows the E_γ spectrum gated on $E_x > 8$ MeV, namely above the neutron separation energy (S_n) at 7414.79 keV. γ -ray energies for known deexcitations [47] from ^{44}Ca and ^{44}K are indicated in the figure as well. One cannot completely exclude very minor contributions from the decay of excited states in ^{44}K (i.e., after proton decay of ^{45}Ca), since some of the energies overlap with deexcitations of states in ^{44}Ca . However, it is clear that the overwhelming majority of transitions observed are from the decay of excited states in ^{44}Ca (i.e., after neutron decay of ^{45}Ca). This indicates that the $(1\nu)(1\pi)^{-1}$ particle-hole states created in the $(t, ^3\text{He})$ reaction predominantly decay by neutron emission.

IV. COMPARISON WITH THEORY

The results are compared with theoretical calculations in Fig. 2. The SM calculations were carried out in the full pf shell-model space with the GXPF1A, KB3G, and FPD6 [23] Hamiltonians using the code NUSHELLX@MSU [48]. The parameters for the GXPF1A interaction have been fitted to reproduce the experimental excitation energies and masses for many pf -shell nuclei. The KB3G interaction is an updated version of the KBF interaction [49], which was used to generate the weak reaction rate library of Refs. [50,51] and whose parameters were primarily deduced from experimental data in the lower pf shell. The FPD6 interaction was derived by taking into account experimental information available for nuclei also in the lower part of the pf shell: $^{41-49}\text{Ca}$, $^{42-44}\text{Sc}$, and ^{44}Ti . These SM calculations have been scaled by a quenching factor of $(0.74)^2$ [52] to account for the shell configurations outside the model space, and have been smeared with the experimental energy resolution of 0.3 MeV (FWHM) in Fig. 2.

All SM calculations associate the bulk of the GT strength with a transition to a state at about 5–6 MeV. Most of the GT strength extracted from the data resides between 3 and 8 MeV, but is much more fragmented than predicted by theory [see Fig. 2(c)]. The summed strength up to an excitation energy of 10 MeV calculated with the FPD6 interaction matches the summed experimental strength extracted from the data quite well, whereas the calculations that employ the KB3G and GXPF1A interactions produce more strength. The summed $B(\text{GT})$ value up to $E_x = 10$ MeV for the FPD6 interactions is $\sum B(\text{GT})_{\text{FPD6}} = 0.38$ (with a further 2.2% of that value located at higher energies) compared to the experimental value of $\sum B(\text{GT}) = 0.38 \pm 0.06(\text{stat.}) \pm 0.03(\text{syst.})$. The summed $B(\text{GT})$ values up to 10 MeV for the GXPF1A and KB3G interactions are $\sum B(\text{GT})_{\text{GXPF1A}} = 0.59$ and $\sum B(\text{GT})_{\text{KB3G}} = 0.47$, respectively, with a further 2.4% and 0.90% of these values located at higher energies.

While the $B(\text{GT})$ value from the β -decay measurement for the transition to the ground state of ^{45}Ca is 3.8×10^{-3} [43], the theoretical values are 0.28×10^{-3} , 0.35×10^{-3} , and 5.5×10^{-3} for the GXPF1A, KB3G, and FPD6 interactions, respectively. Note that the FPD6 interaction gives a value closest to the experiment. The calculated excitation energies of the first $5/2^-$ state, which is located at 174 keV, are 364, 195, and 446 keV for the GXPF1A, KB3G, and FPD6 interactions, respectively, and their $B(\text{GT})$ values are 0.076×10^{-3} , 0.013×10^{-3} , and 0.015×10^{-3} , which are more than two orders of magnitude smaller than the experimental value of $8(5) \times 10^{-3}$.

The large discrepancy between the GT strength distribution extracted from the data and those calculated in the SM using interactions designed for the pf model space was also observed for ^{46}Ti [22]. As described in that reference, the likely cause is the influence of intruder states that involve nucleons excited from the sd shell into the pf shell. A similar discussion on the intruder sd -shell configurations is also found in a recent paper on the β^- charge-exchange measurement on a nearby nucleus ^{44}Ca [53]. There is evidence for such intruder states (see e.g. Ref. [16,54]). It is interesting to note that the SM calculations that employ the FPD6 interaction perform somewhat better

in terms of describing the total GT strength than the SM calculation involving the KB3G and GXPF1A interactions, even though the latter two do rather well in describing GT strengths throughout most of the pf shell. The likely cause is that the FPD6 Hamiltonian was derived by focusing on the experimental data only on the nuclei in the lower part of the pf shell. Consequently, some of the effects of the intruder configurations from the sd shell significantly affected the properties of this Hamiltonian.

According to the SM, the strong transition near 6 MeV in the calculations is from a $5/2^-$ state with the configuration dominated by one neutron in the $f_{5/2}$ orbital. However, due to the proximity to ^{40}Ca core and the excitation of sd -shell nucleons, the level density of $5/2^-$ states is much larger than that obtained in the pf shell alone. In the pf shell there are about six $5/2^-$ states up to 6 MeV in excitation (the $5/2^-$ basis dimension is 253). In the $s_{1/2}$ - $d_{3/2}$ - $f_{7/2}$ - $p_{3/2}$ model space with the Hamiltonian used in Ref. [55] there are about one hundred $5/2^-$ states up to 6 MeV (the $5/2^-$ dimension is 4 215 731). The dimension for a model space that includes $s_{1/2}$, $d_{3/2}$, and pf is too large to consider. Qualitatively, we can interpret the results of the present experiment as a measure of the spreading of the simple pf -shell configuration over the more complex configurations allowed by the excitation of sd -shell nucleons with an observed spreading width of about 2 MeV. To improve GT strength calculations we need to expand the pf shell-model space to include the $0d_{3/2}$ and $1s_{1/2}$ orbitals. The high level density above 5 MeV will require the use of a Lanczos strength function method [56] to obtain the spreading width. The present data, in turn, can be used to benchmark cross-shell effective interactions when they become available.

Also shown in Fig. 2 is the GT distribution based on a QRPA formalism of Ref. [21] using ground-state deformation parameters and masses from the finite-range droplet model of Ref. [57]. This particular model is frequently used for estimating weak-reaction rates in various astrophysical scenarios, primarily because it has the advantage over SM calculations that it can be used across nearly the entire nuclear chart. The theoretical distribution has been smeared with the experimental resolution, but not modified in any other way. Note that in the figure, the theoretical strength distribution has been scaled down by a factor of 3 for visualization purposes. The QRPA calculations also predict a strong GT transition to a state at an excitation energy near 6 MeV, but in addition predict that the strength for the transition to the ground state of ^{45}Ca is more than 30 times larger than the value deduced from the β -decay data.

V. ELECTRON-CAPTURE RATES

Finally, the EC rates (λ_{EC}) based on the experimental and theoretical GT strength distributions were compared. The EC rates were calculated as

$$\lambda_{\text{EC}}(T, \rho) = \ln 2 \sum_j \frac{f_j(T, \rho)}{ft_j}, \quad (2)$$

where f_j is a calculable phase-space factor and ft_j is the comparative half-life. The index j runs over all the states in the daughter nucleus which can be populated through GT

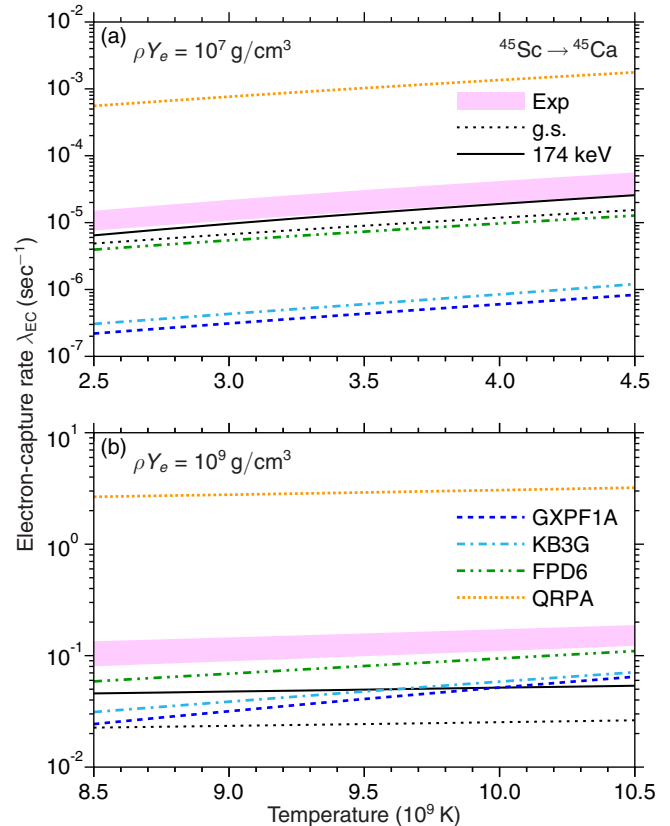


FIG. 4. (Color online) (a) EC rates on ^{45}Ca at $\rho Y_e = 10^7 \text{ g/cm}^3$ as a function of stellar temperatures. The shaded band denotes the EC rate based on the experimental GT strengths (including uncertainties), whereas the dotted and solid lines only represents the EC into the ground and 174-keV states, respectively. The total rates based on the SM (GXPF1A, KB3G, and FPD6) and QRPA calculations are also shown. (b) Same as the one on the top, but at $\rho Y_e = 10^9 \text{ g/cm}^3$.

transitions in the EC reaction. Only transitions from the ground state of the parent nucleus are considered. The calculations were performed as described in Ref. [13] and follow the formalism of Refs. [58–61], implemented in a code previously used in Refs. [8,13].

Figure 4 shows the calculated EC rates at two particular density-temperature combinations: Following Refs. [13,14], these two combinations are $\rho Y_e = 10^7 \text{ g/cm}^3$, $2.5 < T/10^9 \text{ K} < 4.5$ (Case I) as shown in Fig. 4(a), and $\rho Y_e = 10^9 \text{ g/cm}^3$, $8.5 < T/10^9 \text{ K} < 10.5$ (Case II) as shown in Fig. 4(b). Case I corresponds to the conditions during silicon core burning [3], while Case II corresponds to the conditions just prior to the core contraction [4,62], and also to those for the high-density burning regions where EC occurs during the thermonuclear runaway in type Ia SNe [6,7].

The EC rate based on the available experimental information was calculated by combining the $B(\text{GT})$ value for the transition to the ground state from β -decay data with the $B(\text{GT})$ for the transition to the 174-keV state (extracted from the γ -ray analysis in the present data), and the $B(\text{GT})$ distribution to the higher-lying final states from the $(t, ^3\text{He})$ data. In Fig. 4, the EC rates based on the theoretical GT

TABLE I. Deviations between EC rates calculated based on GT strength distributions extracted from charge-exchange experiments and those based on theoretical GT strength distributions, relative to the experimental values, for two stellar density-temperature combinations. The left-hand side of the table refers to deviations for Case I ($\rho Y_e = 10^7 \text{ g/cm}^3$, $T = 3 \times 10^9 \text{ K}$) and the right-hand side of the table refers to those for Case II ($\rho Y_e = 10^9 \text{ g/cm}^3$, $T = 10 \times 10^9 \text{ K}$). The average deviations, as defined in Eq. (3) of the EC rates from the ground states of eight nuclei (^{48}Ti , ^{51}V , ^{56}Fe , $^{58,60,62,64}\text{Ni}$, and ^{64}Zn) in the pf shell, are shown in (a) as presented in Ref. [14]. The deviations for the ^{46}Ti case [22] and the present ^{45}Sc case are shown in (b). The average deviations, with the ^{46}Ti and ^{45}Sc cases included, are shown in (c).

		I: $\rho Y_e = 10^7 \text{ g/cm}^3$, $T = 3 \times 10^9 \text{ K}$			II: $\rho Y_e = 10^9 \text{ g/cm}^3$, $T = 10 \times 10^9 \text{ K}$		
		GXPFI1A	KB3G	QRPA	GXPFI1A	KB3G	QRPA
(a)	$\overline{\Delta_{\text{EC}}}$	-0.25	-0.40	26.	-0.05	0.01	0.54
	$ \overline{\Delta_{\text{EC}}} $	0.31	0.51	27.	0.07	0.27	0.66
(b)	^{46}Ti	-0.61	-0.77	31.	0.17	0.11	4.8
	^{45}Sc	-0.99	-0.98	34.	-0.78	-0.75	19.
(c)	$\overline{\Delta_{\text{EC}}}$	-0.36	-0.50	27.	-0.06	0.11	2.8
	$ \overline{\Delta_{\text{EC}}} $	0.41	0.58	28.	0.09	-0.75	2.9

strength distributions are also shown. The EC rate is very sensitive to the $B(\text{GT})$ distribution at low excitation energies, in particular at lower stellar densities, since the electron Fermi energy at the density of $\rho Y_e = 10^7 (10^9) \text{ g/cm}^3$ is $\epsilon_F(T=0) = 1.2 (5.2) \text{ MeV}$ while $Q_{\text{EC}} = -0.7677 \text{ MeV}$. As shown in Fig. 4, under the lower-density ($\rho Y_e = 10^7 \text{ g/cm}^3$) condition, the EC into the 174-keV state contributes roughly 60% of the total rate at $T = 3.0 \times 10^9 \text{ K}$, while most of the remaining 40% is from the EC into the ground state. The experimental EC rate is larger than those based on the SM calculations due to the difference in the $B(\text{GT})$ distributions at low excitation energies. Among the three SM calculations the one with the FPD6 interaction is the closest to the experimental rate because the FPD6 gives the $B(\text{GT})$ value for the transition to the ground state closest to the experimental data. The experimental EC rate is smaller than that based on the QRPA calculations reflecting the large $B(\text{GT})$ value for the transition to the ground state for the QRPA calculations. These discrepancies might be important in particular in a low density and temperature environment such as presupernova evolution of massive stars [3].

To quantify the differences between the EC rates based on the experimental data and on the theoretical calculations, an average (absolute) deviation $\overline{\Delta_{\text{EC}}}$ ($|\overline{\Delta_{\text{EC}}}|$) was calculated in Refs. [13,14]. These were defined as

$$\overline{\Delta_{\text{EC}}} = \frac{1}{N} \sum_{i=1}^N \frac{\lambda_i^{\text{th}} - \lambda_i^{\text{exp}}}{\lambda_i^{\text{exp}}}, \quad (3a)$$

$$|\overline{\Delta_{\text{EC}}}| = \frac{1}{N} \sum_{i=1}^N \frac{|\lambda_i^{\text{th}} - \lambda_i^{\text{exp}}|}{\lambda_i^{\text{exp}}}, \quad (3b)$$

where λ^{exp} (λ^{th}) is the EC rate based on the experimental data (theory). In Ref. [14], the average was taken for eight nuclei (^{48}Ti , ^{51}V , ^{56}Fe , $^{58,60,62,64}\text{Ni}$, and ^{64}Zn) for which high-resolution data were available, and the summations in Eq. (3) run over these nuclei, namely $N = 8$. In Table I, the average deviations for these eight nuclei for Case I ($\rho Y_e = 10^7 \text{ g/cm}^3$, $T = 3 \times 10^9 \text{ K}$) and those for Case II ($\rho Y_e = 10^9 \text{ g/cm}^3$, $T = 10 \times 10^9 \text{ K}$) are presented together with the deviations

for the present ^{45}Sc case and the recent ^{46}Ti case [22]. The deviations for the two new cases are larger than those for the previous eight cases. Consequently, after combining the two new cases with the previous eight cases, the average deviations between the EC rates deduced from the data and from the theory increases as well.

VI. SUMMARY

We measured the double-differential cross section for the $^{45}\text{Sc}(t, ^3\text{He})$ reaction at 115 MeV/ u and extracted the $B(\text{GT})$ distribution. For the extraction of $B(\text{GT})$ for very weak transitions at low excitation energies, coincidences with γ rays produced in the deexcitation of the residual ^{45}Ca were studied. The extracted $B(\text{GT})$ distribution did not agree with those calculated in the SM by using the GXPFI1A, KB3G, and FPD6 interactions, nor with the results from a QRPA calculation. Consequently, the EC rates calculated based on the theoretical strength distributions also compared unfavorably with the EC rates calculated based on strengths extracted from available experimental data. We conclude that further theoretical improvements are important for providing reliable theoretical predictions of $B(\text{GT})$ and derived EC rates for nuclei in the lower pf -shell nuclei. This is particularly important for astrophysical simulations at relatively low stellar densities, for which transitions to low-lying final states are particularly important.

The measurement in coincidence with γ rays with high resolution has proven to be very useful for extracting transition strengths for very weakly excited states at low excitation energies, since these transitions, even though weak, are important for the astrophysical applications and are even dominant under certain stellar conditions. In the future, this technique can also be applied in studies of unstable isotopes, for which charge-exchange experiments must be performed in inverse kinematics. The GRETINA array will be particularly useful for such studies, since its γ -ray tracking capability provides the necessary position resolution for performing accurate Doppler reconstruction of γ rays produced in-flight.

ACKNOWLEDGMENTS

We thank all the staff at NSCL for their outstanding efforts and support. This work was supported by the U.S. NSF Grant No. PHY-08-22648 (Joint Institute for Nuclear Astrophysics)

and PHY-14-04442. GRETINA was funded by the U.S. DOE Office of Science. Operation of the array at NSCL is supported by NSF under Cooperative Agreement No. PHY-11-02511 (NSCL) and by DOE under Grant No. DE-AC02-05CH11231 (LBNL).

-
- [1] K. Langanke and G. Martínez-Pinedo, Nuclear weak-interaction processes in stars, *Rev. Mod. Phys.* **75**, 819 (2003).
- [2] H. A. Bethe, G. E. Brown, J. Applegate, and J. M. Lattimer, Equation of state in the gravitational collapse of stars, *Nucl. Phys. A* **324**, 487 (1979).
- [3] A. Heger, S. E. Woosley, G. Martínez-Pinedo, and K. Langanke, Presupernova evolution with improved rates for weak interactions, *Astrophys. J.* **560**, 307 (2001).
- [4] W. R. Hix, O. E. B. Messer, A. Mezzacappa, M. Liebendörfer, J. Sampaio, K. Langanke, D. J. Dean, and G. Martínez-Pinedo, Consequences of nuclear electron capture in core collapse supernovae, *Phys. Rev. Lett.* **91**, 201102 (2003).
- [5] H.-Th. Janka, K. Langanke, A. Marek, G. Martínez-Pinedo, and B. Müller, Theory of core-collapse supernovae, *Phys. Rep.* **442**, 38 (2007).
- [6] K. Iwamoto, F. Brachwitz, K. Nomoto, N. Kishimoto, H. Umeda, W. R. Hix, and F.-K. Thielemann, Nucleosynthesis in Chandrasekhar mass models for Type Ia supernovae and constraints on progenitor systems and burning-front propagation, *Astrophys. J. Suppl. Ser.* **125**, 439 (1999).
- [7] F. Brachwitz, D. J. Dean, W. R. Hix, K. Iwamoto, K. Langanke, G. Martínez-Pinedo, K. Nomoto, M. R. Strayer, F.-K. Thielemann, and H. Umeda, The role of electron captures in Chandrasekhar-mass models for Type Ia supernovae, *Astrophys. J.* **536**, 934 (2000).
- [8] S. Gupta, E. F. Brown, H. Schatz, P. Möller, and K.-L. Kratz, Heating in the accreted neutron star ocean: Implications for superburst ignition, *Astrophys. J.* **662**, 1188 (2007).
- [9] H. Schatz, S. Gupta, P. Möller, M. Beard, E. F. Brown, A. T. Deibel, L. R. Gasques, W. R. Hix, L. Keek, R. Lau, A. W. Steiner, and M. Wiescher, Strong neutrino cooling by cycles of electron capture and β^- decay in neutron star crusts, *Nature (London)* **505**, 62 (2014).
- [10] T. N. Tادdeucci, C. A. Goulding, T. A. Carey, R. C. Byrd, C. D. Goodman, C. Gaarde, J. Larsen, D. Horen, J. Rapaport, and E. Sugarbaker, The (p, n) reaction as a probe of beta decay strength, *Nucl. Phys. A* **469**, 125 (1987).
- [11] R. G. T. Zegers *et al.*, Extraction of weak transition strengths via the $(^3\text{He}, t)$ reaction at 420 MeV, *Phys. Rev. Lett.* **99**, 202501 (2007).
- [12] G. Perdikakis *et al.*, Gamow-Teller unit cross sections for $(t, ^3\text{He})$ and $(^3\text{He}, t)$ reactions, *Phys. Rev. C* **83**, 054614 (2011).
- [13] A. L. Cole, T. S. Anderson, R. G. T. Zegers, Sam M. Austin, B. A. Brown, L. Valdez, S. Gupta, G. W. Hitt, and O. Fawwaz, Gamow-Teller strengths and electron-capture rates for pf -shell nuclei of relevance for late stellar evolution, *Phys. Rev. C* **86**, 015809 (2012).
- [14] M. Scott *et al.*, Gamow-Teller transition strengths from ^{56}Fe extracted from the $^{56}\text{Fe}(t, ^3\text{He})$ reaction, *Phys. Rev. C* **90**, 025801 (2014).
- [15] M. Honma, T. Otsuka, B. A. Brown, and T. Mizusaki, Effective interaction for pf -shell nuclei, *Phys. Rev. C* **65**, 061301(R) (2002).
- [16] M. Honma, T. Otsuka, B. A. Brown, and T. Mizusaki, New effective interaction for pf -shell nuclei and its implications for the stability of the $N = Z = 28$ closed core, *Phys. Rev. C* **69**, 034335 (2004).
- [17] M. Honma, T. Otsuka, B. A. Brown, and T. Mizusaki, Shell-model description of neutron-rich pf -shell nuclei with a new effective interaction GXPF1, *Eur. Phys. J. A* **25**, 499 (2005).
- [18] A. Poves, J. Sánchez-Solano, E. Caurier, and F. Nowacki, Shell model study of the isobaric chains $A = 50$, $A = 51$ and $A = 52$, *Nucl. Phys. A* **694**, 157 (2001).
- [19] M. Sasano *et al.*, Gamow-Teller transition strengths from ^{56}Ni , *Phys. Rev. Lett.* **107**, 202501 (2011).
- [20] M. Sasano *et al.*, Extraction of Gamow-Teller strength distributions from ^{56}Ni and ^{55}Co via the (p, n) reaction in inverse kinematics, *Phys. Rev. C* **86**, 034324 (2012).
- [21] P. Möller and J. Randrup, New developments in the calculation of β -strength functions, *Nucl. Phys. A* **514**, 1 (1990).
- [22] S. Noji *et al.*, β^+ Gamow-Teller transition strengths from ^{46}Ti and stellar electron-capture rates, *Phys. Rev. Lett.* **112**, 252501 (2014).
- [23] W. A. Richter, M. G. Van Der Merwe, R. E. Julies, and B. A. Brown, New effective interactions for the $0f1p$ shell, *Nucl. Phys. A* **523**, 325 (1991).
- [24] W. P. Alford, A. Celler, B. A. Brown, R. Abegg, K. Ferguson, R. Helmer, K. P. Jackson, S. Long, K. Raywood, and S. Yen, Measurement of Gamow-Teller and spin dipole strength in the $^{45}\text{Sc}(n, p)^{45}\text{Ca}$ reaction at 198 MeV, *Nucl. Phys. A* **531**, 97 (1991).
- [25] D. J. Morrissey, B. M. Sherrill, M. Steiner, A. Stolz, and I. Wiedenhoever, Commissioning the A1900 projectile fragment separator, *Nucl. Instrum. Methods Phys. Res., Sect. B* **204**, 90 (2003).
- [26] G. W. Hitt, Sam M. Austin, D. Bazin, A. L. Cole, J. Dietrich, A. Gade, M. E. Howard, S. D. Reitzner, B. M. Sherrill, C. Simenel, E. E. Smith, J. Stetson, A. Stolz, and R. G. T. Zegers, Development of a secondary triton beam from primary $^{16,18}\text{O}$ beams for $(t, ^3\text{He})$ experiments at intermediate energies, *Nucl. Instrum. Methods Phys. Res., Sect. A* **566**, 264 (2006).
- [27] B. M. Sherrill *et al.*, Charge-exchange reactions with a secondary triton beam, *Nucl. Instrum. Methods Phys. Res., Sect. A* **432**, 299 (1999).
- [28] M. Berz, K. Joh, J. A. Nolen, B. M. Sherrill, and A. F. Zeller, Reconstructive correction of aberrations in nuclear particle spectrographs, *Phys. Rev. C* **47**, 537 (1993).
- [29] D. Bazin, J. A. Caggiano, B. M. Sherrill, J. Yurkon, and A. Zeller, The S800 spectrograph, *Nucl. Instrum. Methods Phys. Res., Sect. B* **204**, 629 (2003).
- [30] J. Yurkon, D. Bazin, W. Benenson, D. J. Morrissey, B. M. Sherrill, D. Swan, and R. Swanson, Focal plane detector for the S800 high-resolution spectrometer, *Nucl. Instrum. Methods Phys. Res., Sect. A* **422**, 291 (1999).

- [31] S. Paschalis *et al.*, The performance of the Gamma-Ray Energy Tracking In-beam Nuclear Array GRETINA, *Nucl. Instrum. Methods Phys. Res., Sect. A* **709**, 44 (2013).
- [32] B. Bonin, N. Alamanos, B. Berthier, G. Bruge, H. Faraggi, D. LeGrand, J. C. Lugol, W. Mittig, L. Papineau, A. I. Yavin, D. K. Scott, M. Levine, J. Arvieux, L. Farvacque, and M. Buenerd, Response functions of ^{58}Ni , ^{116}Sn and ^{208}Pb to the excitation of intermediate-energy α -particles, *Nucl. Phys. A* **430**, 349 (1984).
- [33] M. Ichimura, H. Sakai, and T. Wakasa, Spin-isospin responses via (p, n) and (n, p) reactions, *Prog. Part. Nucl. Phys.* **56**, 446 (2006).
- [34] J. Cook and J. Carr, Computer program FOLD/DWHI, Florida State University (unpublished); based on F. Petrovich and D. Stanley, Microscopic interpretation of $^7\text{Li} + ^{24}\text{Mg}$ inelastic scattering at 34 MeV, *Nucl. Phys. A* **275**, 487 (1977); modified as described in J. Cook, K. W. Kemper, P. V. Drumm, L. K. Fifield, M. A. C. Hotchkis, T. R. Ophel, and C. L. Woods, $^{16}\text{O}(^7\text{Li}, ^7\text{Be})^{16}\text{N}$ reaction at 50 MeV, *Phys. Rev. C* **30**, 1538 (1984); R. G. T. Zegers, S. Fracasso, and G. Colò (unpublished).
- [35] S. C. Pieper and R. B. Wiringa, Quantum Monte Carlo calculations of light nuclei, *Annu. Rev. Nucl. Part. Sci.* **51**, 53 (2001).
- [36] M. A. Franey and W. G. Love, Nucleon-nucleon t -matrix interaction for scattering at intermediate energies, *Phys. Rev. C* **31**, 488 (1985).
- [37] J. Kamiya *et al.*, Cross section and induced polarization in ^3He elastic scattering at 443 MeV, *Phys. Rev. C* **67**, 064612 (2003).
- [38] S. Y. Van Der Werf, S. Brandenburg, P. Grasduk, W. A. Sterrenburg, M. N. Harakeh, M. B. Greenfield, B. A. Brown, and M. Fujiwara, The effective ^3He -nucleon force in a microscopic DWBA approach to the $(^3\text{He}, t)$ charge-exchange reaction, *Nucl. Phys. A* **496**, 305 (1989).
- [39] K. Miki *et al.*, Identification of the β^+ isovector spin monopole resonance via the ^{208}Pb and $^{90}\text{Zr}(t, ^3\text{He})$ reactions at 300 MeV/ u , *Phys. Rev. Lett.* **108**, 262503 (2012).
- [40] T. Furumoto, Y. Sakuragi, and Y. Yamamoto, Repulsive nature of optical potentials for high-energy heavy-ion scattering, *Phys. Rev. C* **82**, 044612 (2010).
- [41] I. Hamamoto and H. Sagawa, Charge-exchange spin monopole modes, *Phys. Rev. C* **62**, 024319 (2000).
- [42] C. J. Guess *et al.*, The $^{150}\text{Nd}(^3\text{He}, t)$ and $^{150}\text{Sm}(t, ^3\text{He})$ reactions with applications to $\beta\beta$ decay of ^{150}Nd , *Phys. Rev. C* **83**, 064318 (2011).
- [43] M. S. Freedman, F. T. Porter, and F. Wagner, Jr., Low-intensity first-forbidden beta-decay branch in ^{45}Ca , *Phys. Rev.* **140**, B563 (1965).
- [44] T. Burrows, Nuclear data sheets for $A = 45$, *Nucl. Data Sheets* **109**, 171 (2008).
- [45] R. G. T. Zegers *et al.*, The $(t, ^3\text{He})$ and $(^3\text{He}, t)$ reactions as probes of Gamow-Teller strength, *Phys. Rev. C* **74**, 024309 (2006).
- [46] G. W. Hitt *et al.*, Gamow-Teller transitions to ^{64}Cu measured with the $^{64}\text{Zn}(t, ^3\text{He})$ reaction, *Phys. Rev. C* **80**, 014313 (2009).
- [47] J. Chen, B. Singh, and J. A. Cameron, Nuclear data sheets for $A = 44$, *Nucl. Data Sheets* **112**, 2357 (2011).
- [48] B. A. Brown, W. D. M. Rae, E. McDonald, and M. Horoi, NUSHELLX@MSU, <https://people.nslc.msu.edu/~brown/resources/resources.html>
- [49] E. Caurier, K. Langanke, G. Martínez-Pinedo, and F. Nowacki, Shell-model calculations of stellar weak interaction rates. I. Gamow-Teller distributions and spectra of nuclei in the mass range $A = 45$ –65, *Nucl. Phys. A* **653**, 439 (1999).
- [50] K. Langanke and G. Martínez-Pinedo, Shell-model calculations of stellar weak interaction rates: II. Weak rates for nuclei in the mass range $A = 45$ –65 in supernovae environments, *Nucl. Phys. A* **673**, 481 (2000).
- [51] K. Langanke and G. Martínez-Pinedo, Rate tables for the weak processes of pf -shell nuclei in stellar environments, *At. Data Nucl. Data Tables* **79**, 1 (2001).
- [52] G. Martínez-Pinedo, A. Poves, E. Caurier, and A. P. Zuker, Effective g_A in the pf shell, *Phys. Rev. C* **53**, 2602(R) (1996).
- [53] Y. Fujita *et al.*, High-resolution study of $T_z = +2 \rightarrow +1$ Gamow-Teller transitions in the $^{44}\text{Ca}(^3\text{He}, t)^{44}\text{Sc}$ reaction, *Phys. Rev. C* **88**, 014308 (2013).
- [54] G. Stoitcheva, W. Satuła, W. Nazarewicz, D. J. Dean, M. Zalewski, and H. Zduńczuk, High-spin intruder states in the fp -shell nuclei and isoscalar proton-neutron correlations, *Phys. Rev. C* **73**, 061304(R) (2006).
- [55] E. Caurier, K. Langanke, G. Martínez-Pinedo, F. Nowacki, and P. Vogel, Shell model description of isotope shifts in calcium, *Phys. Lett. B* **522**, 240 (2001).
- [56] E. Caurier, G. Martínez-Pinedo, F. Nowacki, A. Poves, and A. P. Zuker, The shell model as a unified view of nuclear structure, *Rev. Mod. Phys.* **77**, 427 (2005), and references therein.
- [57] P. Möller, J. R. Nix, W. D. Myers, and W. J. Swiatecki, Nuclear ground-state masses and deformations, *At. Data Nucl. Data Tables* **59**, 185 (1995).
- [58] G. M. Fuller, W. A. Fowler, and M. J. Newman, Stellar weak interaction rates for sd -shell nuclei. I – Nuclear matrix element systematics with application to ^{26}Al and selected nuclei of importance to the supernova problem, *Astrophys. J. Suppl. Ser.* **42**, 447 (1980).
- [59] G. M. Fuller, W. A. Fowler, and M. J. Newman, Stellar weak interaction rates for intermediate-mass nuclei. II – $A = 21$ to $A = 60$, *Astrophys. J.* **252**, 715 (1982).
- [60] G. M. Fuller, W. A. Fowler, and M. J. Newman, Stellar weak interaction rates for intermediate mass nuclei. III – Rate tables for the free nucleons and nuclei with $A = 21$ to $A = 60$, *Astrophys. J. Suppl. Ser.* **48**, 279 (1982).
- [61] G. M. Fuller, W. A. Fowler, and M. J. Newman, Stellar weak interaction rates for intermediate-mass nuclei. IV – Interpolation procedures for rapidly varying lepton capture rates using effective $\log(ft)$ -values, *Astrophys. J.* **293**, 1 (1985).
- [62] K. Langanke and G. Martínez-Pinedo, Supernova neutrino-nucleus reactions, *Nucl. Phys. A* **731**, 365 (2004).